J. Astrophys. Astr. (2022)43:34
https://doi.org/10.1007/s12036-022-09820-z

BINARIES

Viscous dissipative two-temperature accretion flows around black holes

SHILPA SARKAR and INDRANIL CHATTOPADHYAY*

Aryabhatta Research Institute of Observational Sciences (ARIES), Manora Peak, Nainital 263002, India.
Corresponding author E-mail: indra@aries.res.in

MS received 8 October 2021; accepted 26 January 2022

Abstract. General relativistic, advective, viscous, two-temperature accretion disc solutions are studied around a Schwarzschild black hole. The thermodynamics of the flow is described by the relativistic equation of state or Chattopadhyay and Ryu equation of state modified for a two-temperature regime. The cooling processes considered are bremsstrahlung, synchrotron and the Comptonization of these photons. The degeneracy of accretion solutions in the two-temperature regime is resolved using the so called 'maximum entropy' methodology. Utilizing this method, we analyzed the unique solutions and the corresponding spectra for a broad range of parameter space. Interplay between heating due to viscous dissipation and cooling due to different radiation mechanisms plays a significant role in determining the solution and spectrum obtained. In the end, we analyze the observation of a low luminosity AGN, NGC 3998, fitted using our model.

Keyword. Accretion—two-temperature—black holes—accretion discs—shocks.

1. Introduction

Accretion onto black holes (BH) is the best model to explain luminosity and spectra from active galactic nuclei (AGNs) and microquasars. The first accretion model was proposed by Bondi (1952). Although the disc accretion system was not considered, it served as one of the fundamental models based on which more sophisticated models were developed later. The first accretion disc model was presented by Shakura & Sunyaev (1973). However, it could explain only the thermal bump part of the spectra. The shear between each ring of matter rotating with Keplerian velocities generates viscous stresses, which they consider proportional to the pressure. Viscosity helps in the transport of angular momentum outwards, allowing matter to get accreted towards the central object. However, observationally it cannot account for the hard power-law portion of the spectra. Theoretically, the absence of advection and radial pressure gradient term in the momentum equation in this model are the main drawbacks.

Soon it was understood advection is indeed quite important and should be included for a more general description of the accretion processes (Ichimaru 1977; Liang & Thompson 1980; Fukue 1987; Abramowicz *et al*. 1988; Chakrabarti 1989; Narayan & Yi 1994; Chattopadhyay & Chakrabarti 2011; Chattopadhyay & Kumar 2016). We remember that the matter in the accretion disc around BHs are very hot and are therefore fully ionized. Electrons in such plasma would be radiatively efficient, and heavier ions and/or protons are not. If infall times scales are comparable to cooling time scales, then electrons and protons will not have enough time to thermalize with each other. Therefore, the electrons and positive ions would maintain different temperature distributions or the flow is said to be in the two-temperature regime (Shapiro *et al*. 1976; Colpi *et al*. 1984; Chakrabarti & Titarchuk 1995; Narayan & Yi 1995; Nakamura *et al*. 1996; Rajesh & Mukhopadhyay 2010; Dihingia *et al*. 2018). Many of these models were employed to fit the spectra of various BH candidates (Mandal & Chakrabarti 2008; Yuan & Narayan 2014).

This article is part of the Special Issue on "Astrophysical Jets and Observational Facilities: A National Perspective".

Published online: 07 June 2022

However, in a two-temperature regime, the number of equations are less than the number of variables and therefore, the solutions are degenerate. For a given set of constants of motion, infinite transonic solutions could be obtained. In most of the works done in literature, this degeneracy has not been addressed properly. It was Liang & Thompson (1980) who first identified the degeneracy problem in the two-temperature regime but also made an arbitrary assumption. To quote Liang & Thompson (1980) verbatim '...because of the uncertainty in the mechanism coupling electrons and ions, we simply parameterize T_p/T_e as a constant'. In other words, there is no known mechanism or any guiding principle which may constrain their relationship at any of the boundaries. From then on, every work on two-temperature regime, considered to parameterize T_p/T_e to certain constant values or have forced some relation between them (Shapiro & Salpeter 1975; Yuan & Narayan 2014; Mościbrodzka *et al*. 2016; Sadowski & Gaspari 2017; Sadowski *et al*. 2017; West *et al*. 2017; Chael *et al*. 2019).

However, the degeneracy in a two-temperature regime is irrespective of the type of central object and is generic. In Sarkar & Chattopadhyay (2019a) this issue was addressed for the first time and a maximum entropy methodology was proposed to resolve this degeneracy. They successfully constrained the degeneracy. This entropy maximization principle was extended to other scenarios (Sarkar & Chattopadhyay 2019b; Sarkar *et al*. 2020), where they gave a detailed picture of accretion flows around BHs in a broad range of parameter space as well as analyzed the spectrum. In this paper, we aim for a complete study of relativistic, advective, two-temperature accretion disc but in the presence of viscosity, which was not done before. In the next section, we present the equations of motion then in Section 3, we present the methodology. In Section 4, we present the results, where we discuss the effect of variation of flow parameters on accretion flows. Also, we attempt to model the spectrum of NGC 3998, a nearby galaxy with a supermassive BH at the center. At the end of Section 5, we discuss the outcomes of this work.

2. Mathematical framework and modeling

We study viscous, relativistic accretion disc around Schwarzschild black holes (BH), whose metric is given by

$$ds^2 = g_{tt}c^2dt^2 + g_{rr}dr^2 + g_{\theta\theta}d\theta^2 + g_{\phi\phi}d\phi^2, \quad (1)$$

where $g^{\mu\nu}$s represent the metric tensor components. r, θ and ϕ are the spherical coordinates and t is the time coordinate. We have used the unit system where $G = M_{BH} = c = 1$, where G is the universal gravitation constant, M_{BH} the BH mass and c is the speed of light in vacuum. Furthermore, we assume steady state, axisymmetry and no motion along transverse direction, so $\partial/\partial t = \partial/\partial\phi = \partial/\partial\theta = 0$. Therefore, $-g_{tt} = g_{rr}^{-1} = (1 - 2/r)$ and $g_{\theta\theta} = g_{\phi\phi} = r^2$.

The accretion rate equation is given by

$$\dot{M} = 4\pi u^r \rho r^2 \cos\theta, \quad (2)$$

where ρ is the mass density, u^r is the radial component of the four-velocity and θ is the angle which the flow makes with the transverse direction. $\dot{M}$ is a constant of motion throughout the flow.

The radial momentum balance equation is:

$$u^r\frac{du^r}{dr} + \frac{1}{r^2} - (r-3)u^\phi u^\phi + (g^{rr} + u^r u^r)\frac{1}{e+p}\frac{dp}{dr} = 0, \quad (3)$$

where u^ϕ is the azimuthal component of the four-velocity, p is the local pressure of the accretion flow. The integrated form of the azimuthal component of the momentum balance equation is (Lasota 1994; Sadowski 2009):

$$r^2\rho u^r(l - l_0) = r^2(-u_t)\alpha_v p, \quad (4)$$

where $l = u_\phi$ and l_0 is the value of l at the horizon. The specific angular momentum of the fluid is $\lambda = -u_\phi/u_t = -l/u_t$. Here, α_v is the usual Shakura & Sunyaev (1973) viscosity parameter.

The energy balance equation or the first law of thermodynamics is:

$$u^r\left[\left(\frac{e+p}{\rho}\right)\rho_{,r} - e_{,r}\right] = \Delta Q, \quad (5)$$

where $\Delta Q = Q^+ - Q^-$ is the difference between the heating (Q^+) and cooling (Q^-) rates in the system. Discussion about the dissipative processes has been done in detail in Section 2.2.

2.1 *Equation of state (EoS) and the reduced EoM*

We have considered a system composed of fully ionized plasma, i.e., a collection of protons and electrons. For overall charge neutrality, condition to be satisfied is: $n = n_p = n_{e^-}$. To close the set of equations of motion, we need an equation of state (EoS) describing the fluid.

We have used the Chattopadhyay & Ryu (CR) EoS given by Chattopadhyay (2008) and Chattopadhyay & Ryu (2009). The modified form of this equation for a two-temperature accretion flow is given by (Sarkar & Chattopadhyay 2019a; Sarkar *et al*. 2020):

$$e = n_e m_e c^2 \left(f_e + \frac{f_p}{\eta_{ep}}\right) = \frac{\rho c^2 f}{\tilde{K}}, \tag{6}$$

where

$$f_i = 1 + \Theta_i \left(\frac{9\Theta_i + 3}{3\Theta_i + 2}\right), \quad \Theta_i = \frac{kT_i}{m_i c^2}, \quad \eta_{ep} = \frac{m_e}{m_p}$$

and $\tilde{K} = 1 + 1/\eta_{ep}$. Θ_i is the non-dimensional conjugate of the dimensional temperature (T_i).

⇒ *Differential equation for* Θ_e *and* Θ_p: Equation (5) can be simplified to obtain two differential equations for temperature:

$$\frac{d\Theta_p}{dr} = -\frac{\Theta_p}{N_p}\left(\frac{2r-3}{r(r-2)} + \frac{\gamma_v^2}{v}\frac{dv}{dr}\right) - \mathbb{P}\eta_{ep}, \tag{7}$$

$$\frac{d\Theta_e}{dr} = -\frac{\Theta_e}{N_e}\left(\frac{2r-3}{r(r-2)} + \frac{\gamma_v^2}{v}\frac{dv}{dr}\right) - \mathbb{E}, \tag{8}$$

where N_i are the polytropic indices, $v_r^2 = -u_r u^r/u_t u^t$ and $v^2 = \gamma_\phi^2 v_r^2$. The total Lorentz factor is $\gamma^2 = \gamma_v^2\gamma_\phi^2$; $\gamma_v^2 = (1-v^2)^{-1}$ and the azimuthal Lorentz factor is $\gamma_\phi^2 = \left(1 - v_\phi^2\right)^{-1}$. $\mathbb{P}$ and $\mathbb{E}$ contains information about the dissipative processes of protons and electrons, respectively, the expressions of which are given below:

$$\mathbb{P} = \frac{\Delta Q_p \tilde{K}}{\rho u^r N_p} \quad \text{and} \quad \mathbb{E} = \frac{\Delta Q_e \tilde{K}}{\rho u^r N_e}, \tag{9}$$

where $\Delta Q_i = Q_i^+ - Q_i^-$, and suffix $i = p/e$ stands for protons or electrons, respectively.

⇒ *Differential equation for v*: If we simplify Equation (3), we get the expression for differential equation for velocity, which has the form:

$$\mathcal{D}\frac{dv}{dr} = \mathcal{N}, \tag{10}$$

where

$$\mathcal{N} = -\frac{1}{r(r-2)} + \frac{(r-3)\lambda^2\gamma_\phi^2}{r^4} + a^2\left[\frac{2r-3}{r(r-2)}\right] + \frac{\mathbb{E} + \mathbb{P}\eta_{ep}}{2h\tilde{K}},$$

$$\mathcal{D} = \gamma_v^2\left(v - \frac{a^2}{v}\right).$$

The sound speed (a) is, $a^2 = \mathcal{G}/(h\tilde{K})$, where $\mathcal{G} = \Gamma_p(\Theta_p/\eta_{ep}) + \Gamma_e\Theta_e$ and Γ_is are the adiabatic indices.

Now, we need to simultaneously solve Equations (7), (8) and (10) along with Equations (2) and (4) to obtain the advective accretion solutions.

⇒ On integrating Equation (3), along with the help of all the required equations, we obtain the constant of motion called the generalized Bernoulli constant and is given by,

$$E = h\gamma_v\left(1 - \frac{2}{r}\right)\exp(X_f), \tag{11}$$

where $h = (e+p)/\rho$ is the enthalpy and

$$X_f = \int \frac{\Delta Q_p + \Delta Q_e}{\rho h u^r} - \frac{(r-3)l^2}{(r-2)r^3\gamma_v^2}dr.$$

This generalized Bernoulli constant is a constant of motion throughout the flow, even in the presence of dissipation. In the absence of dissipative processes $X_f = 0$ we obtain the canonical form of Bernoulli constant which is, $E \to \mathcal{E} = -hu_t$ (Lightman *et al*. 1975; Chattopadhyay & Chakrabarti 2011).

2.2 *Dissipative processes*

The heating and cooling terms for protons are:

$$Q_p^+ = \delta_v Q_v + \delta_B Q_B \quad \text{and} \quad Q_p^- = Q_{ep} + Q_{ib}, \tag{12}$$

where Q_v and Q_B are the heating due to viscous and magnetic dissipation, respectively (Ipser & Price 1982; Sadowski 2009). δ, which lies between $0 < \delta < 1$, represents the amount of dissipated heat (viscous or magnetic) transferred to protons, while the rest $(1-\delta)$ is absorbed by electrons. Q_{ep} is the Coulomb coupling or the energy exchange term between electrons and protons. Q_{ib} is the cooling of protons due to inverse bremsstrahlung.

The expressions for heating and cooling of electrons are:

$$Q_e^+ = (1-\delta_v)Q_v + (1-\delta_B)Q_B + Q_{ep} + Q_{comp}$$

and

$$Q_e^- = Q_{br} + Q_{sy} + Q_{cbr} + Q_{csy}, \tag{13}$$

where Q_{comp} is the Compton heating term. Q_{br} and Q_{sy} are the emission due to bremsstrahlung and synchrotron, while their corresponding inverse-Comptonizations are represented by Q_{cbr} and Q_{csy}, respectively. The formulas for measuring these

emissivities are the same as given in Sarkar *et al.* (2020) and Sarkar & Chattopadhyay (2020) and used the references therein.

The expression for heating due to viscous dissipation is given by, $Q_{\rm v} = t^{r\phi}\sigma_{r\phi}$. Formulas for the rest of the above equations are used from Sarkar *et al.* (2020) and Sarkar & Chattopadhyay (2020).

2.3 *Spectral analysis*

The methodology adopted to extract the spectrum is same as in Sarkar *et al.* (2020) (also, see Shapiro 1973). We discuss it in brief below. Suppose j_ν is the isotropic emissivity per unit frequency per unit solid angle in the fluid rest frame. Information of j_ν can be obtained from the emission processes included in the system. In this paper, we have considered bremsstrahlung, synchrotron and their corresponding Comptonizations. Thus, $j_\nu = j_{\nu|\rm br} + j_{\nu|\rm sy} + j_{\nu|\rm cbr} + j_{\nu|\rm csy}$. j_ν are complex functions of temperature and density. For $j_{\nu|sy}$ and $j_{\nu|\rm csy}$, it also depends on the magnetic field. The constants of motion of the system play a role in determining the profile of these variables. First, we need to transform this to a local flat frame which is done by using special-relativistic transformations. Thus, we have

$$j'_{\nu'} = j_\nu \frac{1-v^2}{(1-v\cos\theta')^2} \quad \text{and} \quad \nu' = \nu\frac{\sqrt{1-v^2}}{(1-v\cos\theta')}. \tag{14}$$

Here, θ' is the angle between the direction of the fluid element flowing inwards and the line of sight. We note that some photons emitted from the accretion disc would not reach the observer and captured by the BH itself. This capture angle θ^* depends on the location of photon emission and the expression is given by Zeldovich & Novikov (1971):

$$|\cos\theta^*| = \sqrt{\frac{27}{4}\left(\frac{2}{r}\right)^2\left(\frac{2}{r}\right) + 1}. \tag{15}$$

Hence all photons emitted within this angle will be lost. If we integrate the emissivity given by Equation (14) over the whole volume of the disc and on all solid angles, taking into account θ^*, we get the luminosity of the system per unit frequency interval (L_ν). On plotting this against ν we get the spectrum. We have also included the effect of gravitational redshift, which introduces a factor of $\sqrt{1-2/r}$ in the observed frequency.

The Comptonization of soft photons produces a spectrum which follows a power-law relation and can be represented by $F_\nu \propto \nu^{-\alpha}$, where F_ν is the flux per unit frequency and α is the spectral index. A lower value of α suggests that the spectrum is harder and vice versa.

2.4 *Sonic point conditions and shock conditions*

The flow velocity of the matter very far away from the central BH is generally subsonic ($v < a$). But as the matter is accreted, its kinetic energy increases and the BH boundary condition forces the flow to cross the horizon at the speed of light. Therefore, the flow has to be supersonic ($v > a$) near the central object. Thus, accretion flow is necessarily transonic. Also, from the mathematical point of view, we see from Equation (10) that if at some point of the flow $v = a$, then $\mathcal{D} = 0$ and therefore, $\mathcal{N} = 0$. This location is called the sonic point of the flow ($r_{\rm c}$).

In rotating flows, the system can possess multiple sonic points: inner ($r_{\rm ci}$), middle ($r_{\rm cm}$) and outer ($r_{\rm co}$). $r_{\rm ci}$ and $r_{\rm co}$ are X-type sonic points which are physical in nature and matter can pass through these points, while $r_{\rm cm}$ is unphysical and matter cannot pass through them. In the presence of multiple sonic points, shock may also form. The relativistic shock conditions or the Rankine–Hugoniot conditions (Taub 1948) are obtained from the conservation of mass, energy and momentum flux which are: $[\dot{M}] = 0$, $[\dot{E}] = 0$ and $[\rho h\gamma_v^2 v^2 + P] = 0$, respectively. The square brackets represent the difference between the pre-shock and post-shock quantities.

2.5 *Entropy accretion rate*

The measure of entropy can be obtained by integrating the first law of thermodynamics (Equation 5), by putting the source and sink terms to zero (Kumar *et al.* 2013; Joshi *et al.* 2021). For adiabatic flow, the constant of integration is the measure of entropy, while for a non-adiabatic flow, it varies. However, such an analytical expression cannot be derived in the two-temperature regime because of the presence of $Q_{\rm ep}$ in the energy equation. The measure of entropy can only be computed in a region asymptotically close to the horizon, where we can assume that the effect of gravity is much more than any other interactions (see Sarkar &

Chattopadhyay 2019a,b; Sarkar *et al*. 2020) and the form is given as follows,

$$\dot{\mathcal{M}}_{\rm in} = \sqrt{\exp\left(\frac{f_{\rm ein}-1}{\Theta_{\rm ein}}\right)\exp\left(\frac{f_{\rm pin}-1}{\Theta_{\rm pin}}\right)\Theta_{\rm ein}^{\frac{3}{2}}\Theta_{\rm pin}^{\frac{3}{2}}} \times \sqrt{(3\Theta_{\rm ein}+2)^{\frac{3}{2}}(3\Theta_{\rm pin}+2)^{\frac{3}{2}}u^r_{\rm in}r^2_{\rm in}\cos\theta}, \quad (16)$$

where the subscripts 'in' represents the values asymptotically close to the horizon.

3. Methodology adopted: entropy maximization formulation

The number of Equations (2), (4), (5) and (10) are less than the number of flow variables ($v, l, T_{\rm e}, T_{\rm p}$ and ρ) and hence, infinite solutions are admissible for the same set of constants of motion. In this section, we discuss the principle used to select a unique solution among the multiple transonic solutions obtained. First, (a) we discuss the methodology to obtain a general transonic two-temperature accretion solution and then (b) move on to discuss the entropy maximization methodology used to constrain the degeneracy.

⇒ *Finding a general transonic solution*: For a given set of $\dot{M}$, E, $\alpha_{\rm v}$, $L_0 = h_0 l_0$ and for a particular BH mass ($M_{\rm BH}$), we follow a step by step procedure, to obtain a transonic solution:

1. Select boundary: We select $r_{\rm in}$ ($= 2.001 r_{\rm g}$) asymptotically close to the horizon since near horizon gravity is the most dominant force and supersedes any other form of interactions present.
2. Supply a guess value of proton temperature ($T_{\rm pin}$) at $r_{\rm in}$.
3. For a given value of $T_{\rm pin}$, we supply electron temperature ($T_{\rm ein}$, i.e., $T_{\rm e}$ at $r = r_{\rm in}$).
4. Correspondingly obtain $v_{\rm in}$ for the above value of $T_{\rm ein}$ and $T_{\rm pin}$ from the expression $E \simeq \mathcal{E} = hu_t$. We also obtain the value of $l_0 = L_0/h_0$.
5. Using the above obtained boundary values at $r_{\rm in}$, we integrate the EoM (dv/dr, dl/dr, $d\Theta_{\rm e}/dr$ and $d\Theta_{\rm p}/dr$) and obtain a solution.
6. If the obtained solution is not transonic, or, in other words, does not pass through the sonic point ($r_{\rm c}$) satisfying $\mathcal{N} = \mathcal{D} = 0$, we go to step 3 and iterate on $T_{\rm ein}$ until we obtain a transonic solution. In other words, for a given value of $T_{\rm pin}$ we iterate on $T_{\rm ein}$, to obtain the boundary values at $r_{\rm in}$, and integrate the equations of motion to obtain the transonic solution.

Using the above procedure, we obtain general two-temperature transonic accretion solutions for the supplied set of constants of motion. It may be noted, a particular transonic solution for a given set of constants of motion would correspond only to a particular pair of $T_{\rm pin}$ and $T_{\rm ein}$ values.

⇒ *Finding the unique solution using entropy maximization formulation*: We can conclude from the above methodology that, corresponding to a given value of $T_{\rm pin}$ we have a transonic solution. If we change the value of $T_{\rm pin}$, we get another transonic solution, but still, it corresponds to the same supplied set of constants of motion. Thus, multiple transonic solutions exist. Interestingly, fluid has another parameter to determine the solution preferred by nature, i.e., entropy, and according to the second law of thermodynamics, physical processes prefer those solutions which has a higher entropy. This formulation, proposed earlier by Sarkar & Chattopadhyay (2019a,b) and Sarkar *et al*. (2020) has been utilized in the current work. The two temperature solution possessing the highest entropy is selected. This solution was also found to be more stable than the ones with lower entropy (Sarkar *et al*. 2020).

We explain the above-discussed methodology in Figure 1. We plot the transonic solutions corresponding to the constants of motion $E = 1.001$, $\dot{M} = 0.01\dot{M}_{\rm Edd}$ and constant of integration like $L_0 = 2.4$. The other flow parameters are $\alpha_v = 0.01$, $\beta = 0.01$, $\delta_v = \delta_{\rm B} = 0.5$. The BH mass is 10 $M_\odot$. Here, β is the ratio of the magnetic pressure to gas pressure. Adopting the procedure enumerated before (steps 1–6), we obtain a transonic solution corresponding to a given $T_{\rm pin}$. This has been plotted in Figure 1(a) using Mach number ($M = v/a$) vs r plot. The values of $T_{\rm pin}$ used to obtain the plotted solutions are (1) 3.0×10^{11} K (solid, orange), (2) 5.3×10^{11} K (solid, red), (3) 6.72×10^{11} K (solid, violet), (4) 7.0×10^{11} K (solid, blue) and (5) 7.2×10^{11} K (solid, green). Not only these solutions but infinite such solutions exist corresponding to other values of $T_{\rm pin}$. Among these solutions, some pass through $r_{\rm ci}$, some through $r_{\rm co}$ and some even harbor shock. The corresponding spectra are also unique and have been plotted in Figure 1(b) (following the same color coding as Figure 1a). We compute the bolometric luminosity (L) of all these solutions and present it in Table 1. The corresponding efficiency ($\eta_{\rm R} = L/(\dot{M}c^2)$) is also given in the last column. The efficiency of all these solutions is below 0.07% because the accretion rate of the system is very low. It is interesting to see that both L and $\eta_{\rm R}$

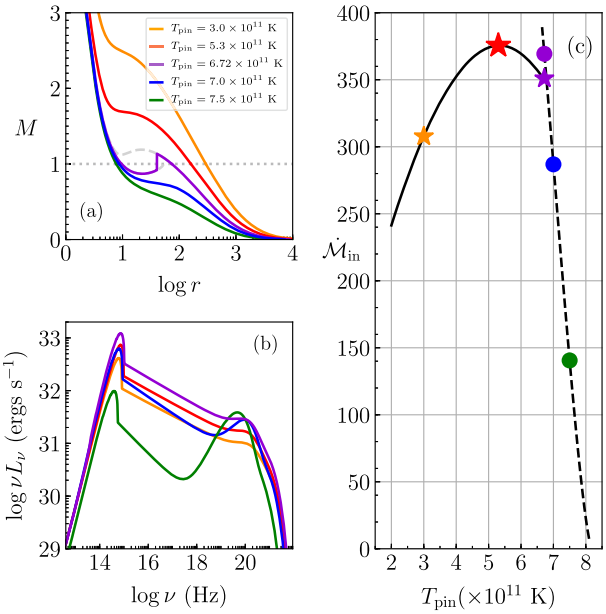

Figure 1. System of degenerate solutions are presented (M vs r plot in panel (a) and the respective spectra in panel (b)). All these correspond to the same set of constants of motion: $E = 1.001$, $\dot{M} = 0.01\dot{M}_{\rm Edd}$ and $M_{\rm BH} = 10\ M_\odot$. The other flow parameters are $L_0 = 2.4$, $\alpha_v = 0.01$, $\beta = 0.01$, $\delta_v = \delta_{\rm B} = 0.5$. In panel (c) the entropy measure of all possible solutions are plotted, as function of $T_{\rm pin}$.

Table 1. Luminosities and efficiencies of different solutions present in Figure 1.

Color code	$T_{\rm pin}$ ($\times 10^{11}$ K)	L ($\times 10^{33}$ ergs s^{-1})	$\eta_{\rm R}$ ($\times 10^{-2}$%)
Orange	3.0	2.164	1.669
Red	5.3	3.586	2.767
Purple	6.72	8.265	6.378
Blue	7.0	5.979	4.614
Green	7.5	0.469	0.362

strongly depend on the solution selected (identified using $T_{\rm pin}$). The solution with $T_{\rm pin} = 6.72 \times 10^{11}$ K (purple curve) is 20 times more luminous than the solution with $T_{\rm pin} = 7.5 \times 10^{11}$ K (green curve). Thus, the selection of a solution is important. This suggests that a serious problem of degeneracy persists in two-temperature accretion flows and hence it is an urgent need to remove it.

Now, in Figure 1(c), we plot the entropy measure ($\dot{\mathcal{M}}_{\rm in}$) using Equation (16) for all the transonic solutions that could be obtained by varying the value of $T_{\rm pin}$ and plot it against the respective $T_{\rm pin}$. The dashed black curve in Figure 1(c) represents parameters for those solutions which pass through $r_{\rm ci}$, while those passing through $r_{\rm co}$ are represented using a solid, black curve. We have marked on the curves, using colored stars and dots, the solutions presented in Figure 1(a).

We find that the entropy maximizes for a particular value of $T_{\rm pin}$, which is 5.3×10^{11} K (red star). Following the second law of thermodynamics, this is the solution that nature would prefer (see Sarkar & Chattopadhyay 2019a,b; Sarkar *et al.* 2020, for details). The corresponding solution and spectra are represented in solid red curves in Figures 1(a) and (b), respectively. The degeneracy can be constrained, and the exact spectra corresponding to the given set of constants of motion can be extracted.

In the rest of the paper by solution, we mean the one with the highest entropy, obtained using the above-described methodology.

4. Results

In all the results presented in this section, we fix the following parameters: $M_{\rm BH} = 10\ M_\odot$, $\delta_v = \delta_{\rm B} = 0.5$, $\beta = 0.01$ and $\theta = 45^\circ$.

4.1 *General viscous dissipative transonic two-temperature accretion disc*

In Figure 2, we plot the solution along with its flow variables for parameters: $E = 1.0005$, $L_0 = 2.9$, $\alpha_v = 0.01$ and $\dot{M} = 0.001\dot{M}_{\rm Edd}$. The solution for this particular set of flow parameters pass through a single $r_{\rm ci}$ and is plotted in Figure 2(a). Below the dotted grey horizontal line (i.e., $M = 1$), the accreting matter is subsonic while above it, matter is supersonic. Also plotted are the flow variables: $\log v$ (Figure 2b), proton and electron temperatures (Figure 2c), l (Figure 2d), number density $\log n$ (Figure 2e) and the adiabatic indices for protons and electrons (Figure 2f). We can conclude from Figure 2(d) that the viscosity is efficient in transporting angular momentum outwards, thus allowing matter to get accreted by the BH. The adiabatic indices, which are representation of the thermal state of the system, varies between 4/3 and 5/3 depending on the temperature as well as the mass of the species (see Figure 2f). This justifies the use of CR EoS, which consistently calculates the $\Gamma_{\rm e}$ and $\Gamma_{\rm p}$ as functions of $T_{\rm e}$ and $T_{\rm p}$, respectively, at each r. Matter is relativistic when $kT_i/(m_i c^2) > 1$. Protons being ~ 1000 times more massive than electrons, tend to remain non-relativistic throughout the flow, even

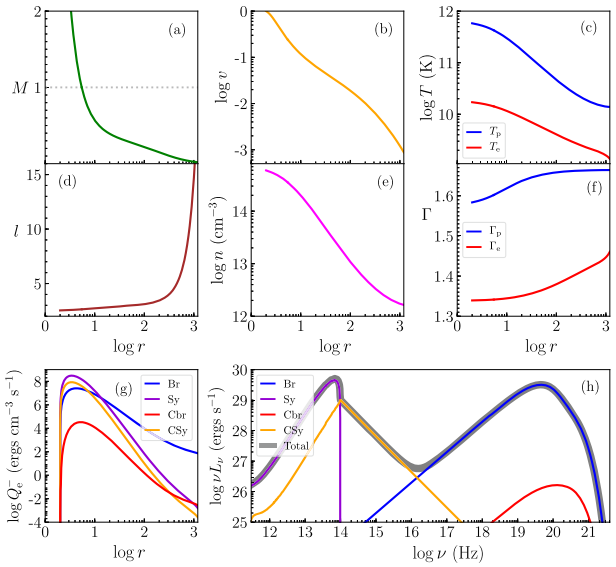

Figure 2. A typical two-temperature accretion solution along with its flow variables and spectrum. The set of flow parameters for this solution are: $E = 1.0005$, $L_0 = 2.9$, $\alpha_v = 0.01$, $\dot{M} = 0.001\dot{M}_{\rm Edd}$ and $M_{\rm BH} = 10\ M_\odot$.

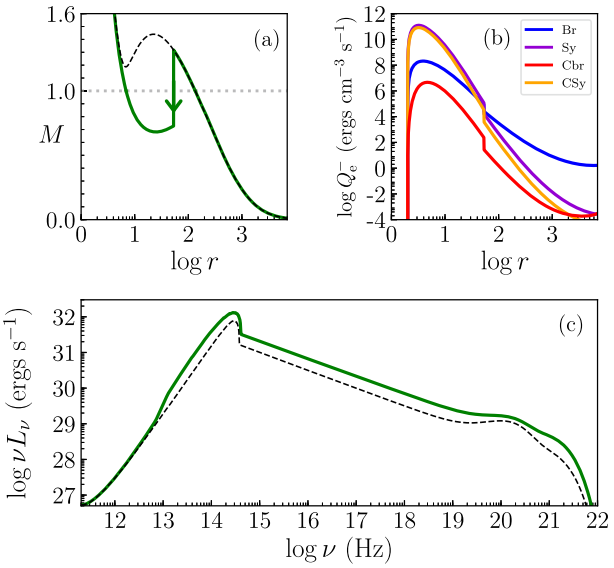

Figure 3. A shocked solution along with its emissivities and spectrum are presented. The set of flow parameters for this solution are: $E = 1.001$, $L_0 = 2.7$, $\alpha_v = 0.01$, $\dot{M} = 0.001\dot{M}_{\rm Edd}$ and $M_{\rm BH} = 10\ M_\odot$. The dashed black curve represents the solution if it had not harbored a shock.

though they possess higher temperatures. On the other hand, electrons become relativistic ($\Gamma_e \sim 1.33$) even at lower temperatures.

In Figure 2(g) we plot the emissivities for various processes like bremsstrahlung ($Q_{\rm br}$, blue), synchrotron ($Q_{\rm sy}$, violet), Comptonized bremsstrahlung ($Q_{\rm cbr}$, red) and Comptonized synchrotron ($Q_{\rm csy}$, orange). We see that bremsstrahlung radiation dominates the majority of the emission coming from the accretion disc with these parameters. It exceeds other radiation processes throughout the flow except for a region $r < 20r_{\rm g}$, where synchrotron emission dominates. The corresponding signatures are distinctly observed in the spectrum presented in Figure 2(h). The bump at higher frequency (blue curve) is obtained from bremsstrahlung, while near $\nu \sim 10^{14}$ Hz, the synchrotron self-absorption peak is prominent. The accretion flow, in this case, is low in energy, and therefore the electrons are moderately hot. This reduces the Comptonization of soft photons significantly, thereby producing a weak power law between 10^{14} Hz $< \nu < 10^{16}$ Hz. Also, it is clear from their corresponding emissivities presented in Figure 2(g) using red and orange curves. Here, it can be seen the total emissivity obtained from both the Comptonization processes is always less than the combined emission from bremsstrahlung and synchrotron. The total spectrum is plotted using a solid black curve in Figure 2(h).

4.2 *Solutions harboring shock*

In Figure 3 we present a two-temperature accretion solution which harbors a shock. The flow parameters are: $E = 1.001$, $L_0 = 2.7$, $\alpha_{\rm v} = 0.01$ and $\dot{M} = 0.001\dot{M}_{\rm Edd}$. A shock is formed due to the combined effect of gravity, centrifugal force and thermal gradient forces and hence depends on the combination of flow parameters used. Across the shock: energy flux, momentum flux and mass flux are all conserved.

Compared to the previous solution (Figure 2), in this case, both the energy and angular momentum are higher. In Figure 3(a), the solution is plotted in the green curve where the shock jump is represented by a downward arrow. The shock location is $r_{\rm sh} = 53.12r_{\rm g}$. On encountering this shock, the supersonic flow becomes subsonic. But this subsonic flow soon gains velocity due to the gravitational attraction of the accretor and again becomes supersonic after passing through $r_{\rm ci}$. If the solution had not harbored a shock, then the solution is that represented by a dashed black curve plotted in the same figure.

The spectrum is plotted in Figure 3(c) for both the solutions: shocked as well as the one without the shock. We see that the solution harboring a shock is overall more luminous. The power-law portion of the spectrum coming due to Comptonization of soft photons increase from $\nu \sim 10^{19}$ Hz (for a solution having no shock) to 4×10^{19} Hz (for a shocked

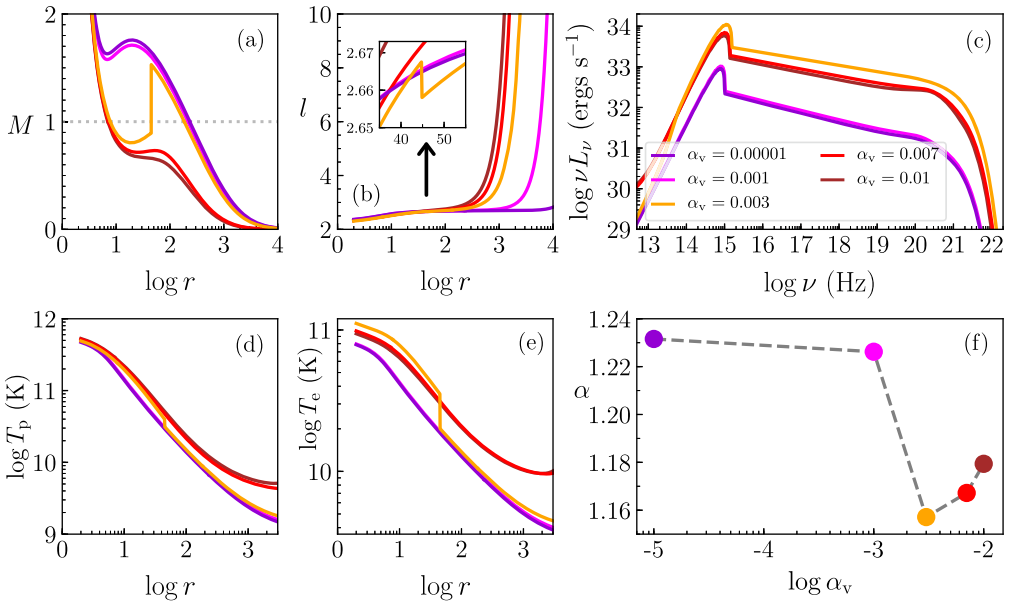

Figure 4. Variation of α_v and its effect on solutions (panel a), l (panel b), spectrum (panel c), T_p (panel d), T_e (panel e) and spectral index (α) (panel f) are presented. The rest of the flow parameters are: $E = 1.001$, $L_0 = 2.7$, $\dot{M} = 0.01\dot{M}_{\rm Edd}$ and $M_{\rm BH} = 10\ M_\odot$.

solution). Also, there is a slight increase in the peak of synchrotron self-absorption frequency. This increase in emission processes is presented in Figure 3(b), where we can see that at the shock jump, there are a sudden increase in the emissivities. Instead of synchrotron emission contributing to the whole emission for $r < 20r_g$, Comptonized synchrotron also becomes comparable.

The spectra presented in both the Figures 2 and 3 are soft because low accretion rate is considered.

An estimate of the QPO frequency: Molteni *et al.* (1996), Chakrabarti *et al.* (2015) and Kim *et al.* (2019) and a host of other works have shown in their numerical simulations that whenever there is a resonance between the infall and cooling timescales, the shock would oscillate at a particular frequency which is comparable with the quasi-periodic oscillation (QPO) frequency. In another argument, it was shown by Das *et al.* (2014) that whenever viscosity exceeds its critical value, the post-shock disc would oscillate. Irrespective of the mechanism triggering oscillation of the post-shock disc, if the shock oscillates, the system is bound to exhibit QPOs (Lee *et al.* 2011; Suková & Janiuk 2015). Although an exact study of the oscillatory nature of the shock would require numerical simulation, we can still estimate the QPO frequency assuming the shock presented in Figure 3 is oscillatory. Following Aktar *et al.* (2017), we compute the QPO frequency for the given system and find it to be around 38.513 Hz. To further investigate the nature of the QPO, we need to perform simulations, which is beyond the scope of the current work.

4.3 *Effect of viscosity: variation of solutions with* α_v

In this section, we study the effect of variation of α_v on the solution and spectra of two-temperature accretion discs. In Figure 4(a), we plot the disc solutions for different values of $\alpha_v = 0.00001$ (violet), 0.001 (magenta), 0.003 (orange), 0.007 (red) and 0.01 (brown). The rest of the flow parameters are: $E = 1.001$, $L_0 = 2.7$ and $\dot{M} = 0.01\dot{M}_{\rm Edd}$. The increase in the value of α_v would proportionally increase the viscous stresses leading to the efficient transport of angular momentum outwards. This could be seen from the l vs r plot given in Figure 4(b). It is evident from the plot that for a solution with very low α_v, the l remains almost constant similar to an inviscid case. It may be noted that, apart from the transport of angular momentum, viscosity leads to heat dissipation in the system. An increase in α_v would correspond to an increase in Q_v, but it would also increase the angular momentum outwards. Higher angular momentum in the outer part would increase the radiation because the rotating matter would increase the infall timescale compared to the cooling timescale. Thus, a combined effect of both heating and cooling will shape the

accretion solution and the corresponding spectrum. While the viscous heat is partly absorbed by protons and partly by electrons, the cooling affects only the electrons. We plot the proton temperature (T_p) in Figure 4(d) and see that there is a gradual increase in the temperature profiles as we increase the α_v. On the other hand, T_e profile (plotted in Figure 4e), shows an increase and then decrease with increasing α_v. The main reason is because of the combined effect of both heating and cooling acting on electrons, as have been discussed previously.

The inner boundary condition is the same for all the flows in this figure. A low α_v solution, as discussed before, admits low angular momentum values throughout the flow, which implies higher radial velocity and hence a smaller infall time scale. Thus the radiative output is low (see violet curves in Figure 4a and c). With increasing α_v we consider flows with higher angular momentum at the outer boundary. Therefore such flows have higher rotation, lower infall velocity. This implies a higher infall timescale causing these flows generally to be more luminous (see, Figure 4c, red and brown curves). But we remember that there is an interplay between heating and cooling processes. Thus, increasing α_v can also make the system less luminous. We find that $L_{\alpha_v=0.01} < L_{\alpha_v=0.007}$. The decrease in L is evident from the T_e profile presented in Figure 4(e) (brown curve). For intermediate values of α_v, in this case for $\alpha_v = 0.003$, the system harbors a shock. The shocked solution is found to be the most luminous as well as harder than the rest of the solutions due to its hotter post-shock flow.

We plot the spectral index (α) of the power-law component, corresponding to the spectra presented in Figure 4(c). A lower value of α corresponds to a harder spectrum and vice-versa. It is seen that the low luminous systems are softer. The shocked solution with $\alpha = 1.157$ is the hardest of all the spectra presented. This is due to the increased inverse-Comptonization in the hotter post-shock flow.

4.4 *Importance of accretion rate of a system*

In this section, we discuss the effect of varying accretion rate (see Figure 5) on the observational properties like (a) spectrum, (b) bolometric luminosity (L), (c) efficiency (η_R) and (d) spectral index (α). The values of accretion rate used for this purpose are: $0.001\dot{M}_{Edd}$ (solid, red), $0.01\dot{M}_{Edd}$ (solid, orange) and $0.1\dot{M}_{Edd}$ (solid, green). The other flow parameters are: $E = 1.0005$, $L_0 = 2.4$ and $M_{BH} = 10\ M_\odot$. In Figure 5(b), we see that with the increase in $\dot{M}$, the

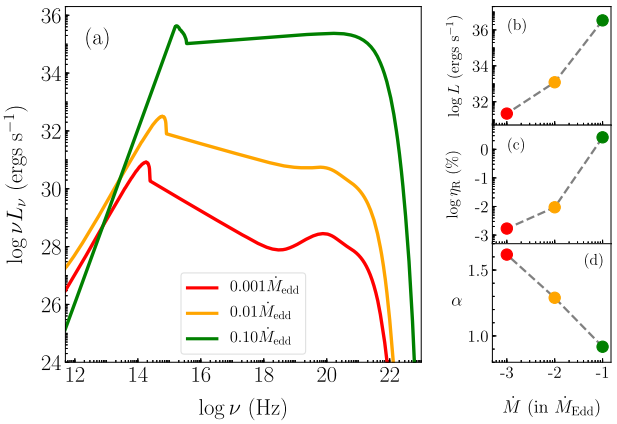

Figure 5. Effect of accretion rate ($\dot{M}$) on (a) spectrum, (b) bolometric luminosity (L), (c) efficiency (η_R) and (d) spectral index (α). Accretion rate values varied are $0.001\dot{M}_{Edd}$ (solid, red), $0.01\dot{M}_{Edd}$ (solid, orange) and $0.1\dot{M}_{Edd}$ (solid, green). The rest of the flow parameters are: $E = 1.0005$, $L_0 = 2.4$ and $M_{BH} = 10\ M_\odot$.

luminosity increases. This is because a higher accretion rate implies the accretion of more matter, or in other words, higher number density. This increase in n enhances the cooling processes leading to high luminosities. Figure 5(c) plots the corresponding efficiencies defined by $\eta_R = L/(\dot{M}c^2)$. For low accretion rates, the efficiency of conversion of matter into radiation is less. With the increase in $\dot{M}$ the efficiency increases and for $0.1\dot{M}_{Edd}$ it is $\sim 2.622\%$. Thus, this plot concludes that the efficiency of a BH accretion system is not constant and depends on $\dot{M}$. Spectral indices (α) are plotted in Figure 5(d). With the increase in $\dot{M}$ the spectrum becomes harder due to the additional inverse-Comptonization caused by the excess number density of electrons.

4.5 *Modeling NGC 3998 spectrum*

NGC 3998 is a S0 galaxy located at a distance of 13.1 Mpc (Maoz 2007) with a central BH mass $\sim 10^{8.9}\ M_\odot$ (Nemmen *et al.* 2010; Bandyopadhyay *et al.* 2019). This galaxy has been well studied with various instruments like Swift, XMM-Newton, NuSTAR and BeppoSAX. We used the data present in Nemmen *et al.* (2010), Ptak *et al.* (2004), Bandyopadhyay *et al.* (2019) and references therein. We plot these data points using grey stars in Figure 6. It may be noted that the quasi-simultaneous X-ray data presented above show very little evidence of outflow activity from the source, nor much

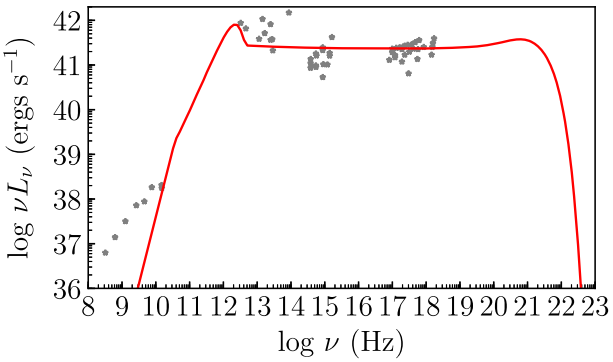

Figure 6. Modeling of NGC 3998 spectrum.

evidence of non-thermal electrons have been found (Bandyopadhyay *et al*. 2019). Since the accretion flow, we considered is composed of plasma where the particles follow relativistic Maxwell distribution and without any mass loss, NGC 3998 seems a good candidate in which our model could be applied to explain the data.

The model spectrum (red, solid) fits reasonably well in the X-ray band. The accretion flow parameters for this fit are $\dot{M} = 0.0075\dot{M}_{\rm Edd}$, $\beta = 0.45$, $L_0 = 2.4$, $\alpha_{\rm v} = 0.004$, $E = 1.005$. The bolometric luminosity is $L \sim 6.052 \times 10^{42}$ ergs s^{-1} and emission in the range 2–10 keV is $L_X = 3.729 \times 10^{41}$ ergs s^{-1}, which agrees well with the estimation from observations. The hump in the IR range is from the synchrotron emission. While the data points in the radio might be a contribution of some outflows. It may be noted that the data in the X-rays and that in the lower energy bands presented here are not simultaneous, and hence we concentrated only on the X-ray band. Further, the fitting is done by eye estimation as was done by other authors Ptak *et al*. (2004), Nemmen *et al*. (2010) and Bandyopadhyay *et al*. (2019). This fitting can be made better with simultaneous broadband data and one can impose a tighter constraint on the accretion disc parameters.

5. Discussion and concluding remarks

In this paper, we have studied viscous, general relativistic, advective accretion flow onto a non-rotating BH in the two-temperature regime. In addition, we have used an approximate, relativistic equation of state to describe the fluid. We employed the entropy maximization method to compute the unique accretion solution, otherwise a degenerate set of equations. It is probably for the first time we employed the entropy maximization technique to obtain a unique viscous transonic solution.

The removal of degeneracy and obtaining a unique solution is necessary. A wrong solution and spectra, if selected, might mislead us, and we can arrive at a different conclusion for the given system. This work, in addition to Sarkar & Chattopadhyay (2019a,b) and Sarkar *et al*. (2020) used the first principles instead of arbitrary parametrizations to constrain the degeneracy and obtain a unique two-temperature accretion solution. The second law of thermodynamics was the guiding principle, which dictated that a solution with the maximum entropy is the one which nature would prefer the most.

This methodology was followed throughout the paper to obtain solutions and thereby analyze the spectra. We showed that the accretion disc solution depends on viscosity. Higher viscosity implies stronger angular momentum transport and hence more luminous flows are expected. We also showed that a shocked solution is hotter and more luminous than the solution if it had not harbored a shock. Shock signatures in flow variables are always present. While flow velocity becomes subsonic, temperatures, l, n and emissivities jump to higher values. This makes the spectra harder. If such a shock is oscillatory, then QPOs would form. But for investigating the oscillatory nature of the shock, numerical simulations need to be performed, which is beyond the scope of the current work.

The use of CR EoS removed the constraint of fixing adiabatic indices. The value of Γ represent the thermal state of the matter which in turn not only depends on T but also on mass. The implementation of CR EoS for multispecies flow is necessary to compute the adiabatic indices consistently at every r.

We concluded that the efficiency and spectral index of a system depends on the heating and cooling processes present in the system. An increase in accretion rate increases the cooling because of the supply of more matter. A low accretion rate system have low radiative efficiencies and softer spectra. With the increase in $\dot{M}$, $\eta_{\rm R}$ increases and the spectra become harder. Change in viscosity affects both the heating and cooling of the system. While the increase in viscosity increases angular momentum outwards, allowing more time for the matter to radiate, it also enhances heating. Thus, increasing $\alpha_{\rm v}$ makes the spectrum harder initially, but further increase might make it softer.

We also modeled the NGC 3998 spectrum and found that the obtained luminosities are consistent

with that got in the literature. We aim to investigate this object in greater detail using an additional jet component to fit the radio emission. Also, the current model needs to implement emissions from non-thermal electrons. We keep this work to be attended in future.

Acknowledgement

We thank the anonymous referee for giving suggestions which improved the quality of the paper further.

References

Abramowicz M. A., Czerny B., Lasota J. P., Szuszkiewicz E., 1988, ApJ, 332, 646. https://doi.org/10.1086/166683
Aktar R., Das S., Nandi A., Sreehari H., 2017, MNRAS, 471, 4806. https://doi.org/10.1093/mnras/stx1893
Blaes O., 2014, SSRv, 183, 21. https://doi.org/10.1007/s11214-013-9985-6
Bondi H., 1952, MNRAS, 112, 195. https://doi.org/10.1093/mnras/112.2.195
Bandyopadhyay B., Xie F.-G., Nagar N. M., *et al.*, 2019, MNRAS, 490, 4606. https://doi.org/10.1093/mnras/stz2874
Chael A., Narayan R., Johnson M. D., 2019, MNRAS, 486, 2873. https://doi.org/10.1093/mnras/stz988
Chakrabarti S. K., 1989, ApJ, 347, 365. https://doi.org/10.1086/168125
Chakrabarti S., Titarchuk L. G., 1995, ApJ, 455, 623. https://doi.org/10.1086/176610
Chakrabarti S. K., Mondal S., Debnath D., 2015, MNRAS, 452, 3451. https://doi.org/10.1093/mnras/stv1566
Chattopadhyay I., 2008, AIPC, 1053, 353. https://doi.org/10.1063/1.3009507
Chattopadhyay I., Ryu D., 2009, ApJ, 694, 492. https://doi.org/10.1088/0004-637X/694/1/492
Chattopadhyay I., Chakrabarti S. K., 2011, IJMPD, 20, 1597. https://doi.org/10.1142/S0218271811019487
Chattopadhyay I., Kumar R., 2016, MNRAS, 459, 3792. https://doi.org/10.1093/mnras/stw876
Colpi M., Maraschi L., Treves A., 1984, ApJ, 280, 319. https://doi.org/10.1086/161998
Das S., Chattopadhyay I., Nandi A., Molteni D., 2014, MNRAS, 442, 251. https://doi.org/10.1093/mnras/stu864
Di Matteo T., Quataert E., Allen S. W., Narayan R., Fabian A. C., 2000, MNRAS, 311, 507. https://doi.org/10.1046/j.1365-8711.2000.03134.x
Dihingia I. K., Das S., Mandal S., 2018, MNRAS, 475, 2164. https://doi.org/10.1093/mnras/stx3269
Fukue J., 1987, PASJ, 39, 309
Ichimaru S., 1977, ApJ, 214, 840. https://doi.org/10.1086/155314
Ipser J. R., Price R. H., 1982, ApJ, 255, 654. https://doi.org/10.1086/159866
Joshi R. K., Chattopadhyay I., Yadav L., 2021, MNRAS. https://doi.org/10.1093/mnras/stab2841
Kim J., Garain S. K., Chakrabarti S. K., Balsara D. S., 2019, MNRAS, 482, 3636. https://doi.org/10.1093/mnras/sty2953
Kumar R., Singh C. B., Chattopadhyay I., Chakrabarti S. K., 2013, MNRAS, 436, 2864. https://doi.org/10.1093/mnras/stt1781
Lasota J. P., 1994, ASIC, 417, 341
Lee S.-J., Ryu D., Chattopadhyay I., 2011, ApJ, 728, 142. https://doi.org/10.1088/0004-637X/728/2/142
Liang E. P. T., Thompson K. A., 1980, ApJ, 240, 271. https://doi.org/10.1086/158231
Lightman A. P., Press W. H., Price R. H., Teukolsky S. A., 1975, pbrg.book
Mandal S., Chakrabarti S. K., 2008, ApJL, 689, L17. https://doi.org/10.1086/595782
Manmoto T., Mineshige S., Kusunose M., 1997, ApJ, 489, 791. https://doi.org/10.1086/304817
Maoz D., 2007, MNRAS, 377, 1696. https://doi.org/10.1111/j.1365-2966.2007.11735.x
Molteni D., Sponholz H., Chakrabarti S. K., 1996, ApJ, 457, 805. https://doi.org/10.1086/176775
Mościbrodzka M., Falcke H., Noble S., 2016, A&A, 596, A13. https://doi.org/10.1051/0004-6361/201629157
Nakamura K. E., Matsumoto R., Kusunose M., Kato S., 1996, PASJ, 48, 761. https://doi.org/10.1093/pasj/48.5.761
Narayan R., Yi I., 1994, ApJL, 428, L13. https://doi.org/10.1086/187381
Narayan R., Yi I., 1995, ApJ, 452, 710. https://doi.org/10.1086/176343
Nemmen R., Storchi-Bergmann T., Eracleous M., Yuan F., 2010, IAUS, 267, 313. https://doi.org/10.1017/S1743921310006538
Ptak A., Terashima Y., Ho L. C., Quataert E., 2004, ApJ, 606, 173. https://doi.org/10.1086/382940
Rajesh S. R., Mukhopadhyay B., 2010, MNRAS, 402, 961. https://doi.org/10.1111/j.1365-2966.2009.15925.x
Sadowski A., 2009, ApJS, 183, 171. https://doi.org/10.1088/0067-0049/183/2/171
Sadowski A., Gaspari M., 2017, MNRAS, 468, 1398. https://doi.org/10.1093/mnras/stx543
Sadowski A., Wielgus M., Narayan R., *et al.* 2017, MNRAS, 466, 705. https://doi.org/10.1093/mnras/stw3116
Sarkar S., Chattopadhyay I., 2019a, IJMPD, 28, 1950037. https://doi.org/10.1142/S0218271819500378
Sarkar S., Chattopadhyay I., 2019b, JPhCS, 1336, 012019. https://doi.org/10.1088/1742-6596/1336/1/012019
Sarkar S., Chattopadhyay I., 2020, JPhCS, 1640, 012022. https://doi.org/10.1088/1742-6596/1640/1/012022
Sarkar S., Chattopadhyay I., Laurent P., 2020, A&A, 642, A209. https://doi.org/10.1051/0004-6361/202037520
Shakura N. I., Sunyaev R. A., 1973, A&A, 500, 33

Shapiro S. L., Lightman A. P., Eardley D. M., 1976, ApJ, 204, 187. https://doi.org/10.1086/154162
Shapiro S. L., 1973, ApJ, 180, 531. https://doi.org/10.1086/151982
Shapiro S. L., Salpeter E. E., 1975, ApJ, 198, 671. https://doi.org/10.1086/153645
Suková P., Janiuk A., 2015, MNRAS, 447, 1565. https://doi.org/10.1093/mnras/stu2544
Taub A. H., 1948, PhRv, 74, 328. https://doi.org/10.1103/PhysRev.74.328
West B. F., Wolfram K. D., Becker P. A., 2017, ApJ, 835, 129. https://doi.org/10.3847/1538-4357/835/2/129
Yuan F., Narayan R., 2014, ARA&A, 52, 529. https://doi.org/10.1146/annurev-astro-082812-141003
Zeldovich Y. B., Novikov I. D., 1971, reas.book